JEE Journal of Ecological Engineering

Journal of Ecological Engineering, 2026, 27(6), 336–350
https://doi.org/10.12911/22998993/216148
ISSN 2299–8993, License CC-BY 4.0

Received: 2025.09.30
Accepted: 2026.04.16
Published: 2026.05.01

Linking pollutant removal, water quality, and methane emissions in palm oil mill effluent ponds

Amir Noviyanto[1], Valensi Kautsar[1*], Yovi Avianto[1], Sri Gunawan[1], Yohana Theresia Maria Astuti[1], Siti Maimunah[2], Fadhlullah Ramadhani[3]

[1] Department of Agrotechnology, Faculty of Agriculture, Stiper Agricultural University, Yogyakarta, Indonesia
[2] Department of Forestry, Faculty of Forestry, Stiper Agricultural University, Yogyakarta, Indonesia
[3] Research Center for Geoinformatics, Research Organization for Electronics and Informatics, National Research and Innovation Agency, Bandung, Indonesia
* Corresponding author's: valkauts@instiperjogja.ac.id

ABSTRACT

Palm oil mill effluent (POME) treatment ponds play a dual role in pollutant removal and greenhouse gas (GHG) emissions. This study examines the relationship between water quality parameters and methane (CH_4) fluxes across a tropical multi-pond POME treatment system operating under continuous loading. Field monitoring was conducted along a sequential anaerobic–facultative–aerobic pond train, measuring CH_4 fluxes and key physicochemical parameters, including chemical oxygen demand (COD), total suspended solids (TSS), and ammonia nitrogen (NH_3–N). Results revealed a pronounced spatial gradient, with CH_4 flux decreasing from 4,931.3 mg m^{-2} h^{-1} in the early anaerobic pond to 2,758.5 mg m^{-2} h^{-1} in the final polishing pond, indicating a transition from methanogenic to more oxidative conditions. Multivariate regression analysis identified ammonia ($R^2 = 0.68$, $p < 0.01$) and TSS ($R^2 = 0.54$, $p < 0.05$) as strong positive predictors of CH_4 emissions, whereas COD exhibited a significant negative association ($R^2 = –0.47$, $p < 0.05$). These results suggest that methane emissions are more closely linked to substrate bioavailability and nitrogen-mediated microbial processes than to total organic load alone. Elevated ammonia concentrations likely reflect active ammonification and enhanced buffering conditions that favor methanogenesis, while non-biodegradable COD fractions and acidification may constrain CH_4 production. This study provides new insight by highlighting ammonia as a key predictor of methane emissions and by demonstrating a non-linear relationship between organic load and GHG release in tropical POME pond systems. Integrating pollutant removal efficiency with emission mitigation strategies – such as controlled aeration, biofilm enhancement, and nitrogen management – is therefore essential for sustainable POME treatment.

Keywords: palm oil mill effluent, methane emissions, ammonia nitrogen, open pond systems, greenhouse gas mitigation.

INTRODUCTION

Palm oil production remains a major agro-industrial driver in tropical economies, particularly Indonesia and Malaysia, while simultaneously generating large volumes of palm oil mill effluent (POME) – a high-strength wastewater enriched in organic matter, suspended solids, and nitrogenous compounds. When inadequately managed, POME poses substantial risks to aquatic ecosystems and can undermine regional environmental performance metrics, particularly in rapidly expanding production landscapes (Kacaribu et al., 2025). The dominant treatment approach in many mills is a multi-stage open-pond system due to its operational simplicity and low capital cost; however, ponding systems are land-intensive and can act as persistent hotspots of methane (CH_4) emissions during anaerobic processing stages (Mahapatra et al., 2022).

Methane emissions from POME ponds arise primarily from anaerobic decomposition of labile organic substrates and subsequent methanogenesis, and therefore represent an important

climate-relevant externality of wastewater management. Recent syntheses of POME treatment technologies emphasize that conventional pond systems, although effective for reducing bulk pollutants, may release significant CH_4 unless emission control (e.g., biogas capture, engineered oxidation zones, or hybrid upgrades) is implemented (Dominic and Baidurah, 2022; Khan et al., 2025). Moreover, techno-economic and sustainability-focused assessments increasingly frame POME treatment not only as an effluent compliance challenge but also as a resource recovery and ESG issue, where methane control can strongly influence overall environmental outcomes (Junaidi et al., 2025).

Although CH_4 formation is often discussed as a function of organic loading, emerging evidence indicates that methane dynamics in high-strength wastewaters are regulated by multiple interacting water-quality controls. Chemical oxygen demand (COD) represents total oxidizable organic matter, but its relationship with methane is frequently non-linear because COD aggregates chemically distinct fractions with different biodegradability and fermentation pathways. In POME, bulk COD can be conceptualized as a mixture of (i) readily biodegradable soluble COD that rapidly ferments into volatile fatty acids (VFAs), (ii) slowly biodegradable particulate COD associated with suspended solids and requiring hydrolysis, and (iii) inert/refractory COD that is poorly convertible under anaerobic conditions. Consequently, methane generation is expected to track the bioavailable fraction rather than total COD alone, and systems may display inverse or weak COD–CH_4 relationships when refractory fractions dominate or when rapid acidogenesis transiently suppresses methanogens (e.g., via VFA accumulation and pH depression) (Li et al., 2024).

Total suspended solids (TSS) can further amplify methanogenesis by providing particulate substrates and protective micro-niches that sustain anaerobic consortia. Suspended solids also prolong hydrolysis–fermentation sequences, potentially increasing precursor availability for methane formation in upstream ponds. In parallel, nitrogen transformations can play a central regulatory role. Ammonia nitrogen (NH_3–N / NH_4^+–N) is a proxy for protein degradation and ammonification, and it can influence buffering capacity and microbial community function. Recent anaerobic digestion studies and reviews highlight that nitrogen availability and ammonia stress/selection can shift methanogenic pathways and process stability, underscoring the need to explicitly consider dissolved nitrogen when interpreting methane dynamics in high-organic-load systems (Kumar et al., 2022; Chen et al., 2024). In addition, contemporary POME research increasingly explores process upgrades that couple pollutant removal with biological transformation pathways (including algal–bacterial systems), reinforcing that water-quality evolution and methane formation are tightly coupled within pond ecologies (Djarot et al., 2024).

Despite this progress, the coupled behavior of COD, TSS, and NH_3–N as predictors of CH_4 flux across sequential pond stages (anaerobic → facultative → maturation) remains insufficiently resolved for tropical POME pond trains. In particular, few field studies explicitly test whether nitrogen-linked indicators can outperform bulk COD as predictors of methane hotspots along the treatment gradient. To address this gap, the present study integrates spatially resolved CH_4 flux measurements (floating closed chamber) with concurrent water-quality monitoring to quantify how COD, TSS, and NH_3–N jointly regulate methane emissions across distinct functional ponds. By linking pollutant removal performance, water-quality transformations, and methane flux dynamics, this work provides a process-oriented basis for low-emission POME management strategies that align treatment efficiency with climate mitigation objectives.

MATERIALS AND METHODS

Study site and experimental design

This study was conducted at a full-scale palm oil mill effluent (POME) treatment facility operated by PT. XYZ in Central Kalimantan, Indonesia. The facility employs a conventional open-pond treatment system operated under continuous-flow conditions, consisting of a series of anaerobic, facultative, and maturation ponds arranged sequentially to achieve progressive reductions in organic load and suspended solids prior to discharge. Such pond-based systems remain the dominant POME treatment technology in tropical palm oil–producing regions due to their operational simplicity and low energy demand.

To capture spatial variability along the treatment train, four representative ponds were selected based on their functional roles within the system: Pond 1 (raw influent receiving pond), Pond 2 (early anaerobic stage with high organic

loading), Pond 5 (intermediate pond reflecting partial stabilization), and Pond 8 (final polishing pond characterized by lower organic load and increased oxidation potential). This selection was designed to represent a longitudinal gradient in redox conditions, substrate availability, and microbial activity, thereby enabling assessment of how methane emissions and water quality evolve across successive treatment stages.

Within each pond, three sampling locations were established along the main flow path (inlet, center, and outlet) to account for spatial heterogeneity in physicochemical conditions and gas exchange processes. Field measurements were conducted during the morning period (08:00–10:00 local time) under relatively stable meteorological conditions in order to minimize the influence of short-term diurnal variability on methane flux estimates. Methane flux measurements and water-quality sampling were performed concurrently at each location to ensure direct linkage between emission dynamics and effluent characteristics at the time of observation.

Pond geometry and hydraulic context

To support a process-based interpretation of methane emissions under continuous-flow operation, pond geometry was quantified using GIS-derived planimetric measurements. Pond surface areas (A, m²) were delineated from georeferenced pond polygons, yielding 3,315.78 m² (Pond 1), 2,184.41 m² (Pond 2), 6,349.85 m² (Pond 5), and 8,641.35 m² (Pond 8). During the monitoring period, the ponds operated at a relatively stable mean water depth of 4 m, consistent with routine facility operation.

Operational pond volumes (V, m³) were estimated as a function of surface area and mean water depth according to:

$$V = A \times H \tag{1}$$

where: H is the mean water depth (m).

Based on this relationship, estimated operational volumes were 13,263.12 m³ (Pond 1), 8,737.64 m³ (Pond 2), 25,399.40 m³ (Pond 5), and 34,565.40 m³ (Pond 8) (Table 1).

Because the treatment train operates under continuous-flow conditions, hydraulic retention time (HRT, days) is conceptually defined as:

$$HRT = \frac{V}{Q} \tag{2}$$

where: Q is the average inflow rate (m³ d⁻¹).

Although detailed flow records were not available for all ponds during the sampling window, this formulation is provided to frame the role of pond geometry and hydraulic regime in regulating treatment progression and methane dynamics. Differences in pond surface area and volume imply variations in buffering capacity, potential retention time, and gas exchange area, which are critical factors influencing methane production and emission at the pond scale.

Surface loading framework

Under continuous-flow operation, areal (surface) loading rates provide a mechanistic descriptor of substrate delivery to stabilization ponds and are commonly used to interpret biological process intensity in pond-based treatment systems. For any water-quality parameter x (COD, TSS, or NH_3–N), the areal loading rate (Lx, g m⁻² d⁻¹) is defined as:

$$L_x = \frac{Q \times C_x}{A} \tag{3}$$

where: C_x is the measured concentration (g m⁻³),
Q is the average inflow rate (m³ d⁻¹), and
A is the pond surface area (m²).

Areal loading integrates hydraulic input, substrate concentration, and pond geometry, and therefore provides a more process-relevant metric than concentration alone for interpreting anaerobic activity and methane formation.

In the present study, detailed flow records (Q) were not available for all ponds during the

Table 1. GIS-derived pond geometry and derived operational volumes (mean depth = 4 m)

Pond	Functional stage	Surface area, A (m²)	Mean depth, H (m)	Estimated volume, V (m³)
Pond 1	Raw influent / upstream	3,315.78	4.0	13,263.12
Pond 2	Early anaerobic	2,184.41	4.0	8,737.64
Pond 5	Intermediate	6,349.85	4.0	25,399.40
Pond 8	Final polishing	8,641.35	4.0	34,565.40

monitoring period; therefore, areal loading rates are presented as a conceptual framework rather than as fully quantified variables. This formulation is used to support interpretation of emission patterns by highlighting that methane fluxes are expected to respond to the rate of bioavailable substrate delivery per unit area and effective retention conditions, rather than to bulk water-quality concentrations alone. Accordingly, pond geometry-scaled metrics (e.g., pond-wide methane emissions) are employed to complement flux-based analyses.

Methane flux measurement

Methane emissions were quantified using the floating closed chamber technique, a widely applied method for estimating gas fluxes at the water–air interface in aquatic and wetland ecosystems (Rocher-Ros et al., 2023). The chamber was constructed from transparent acrylic with dimensions of 50 × 50 × 50 cm, providing a headspace volume of approximately 125 L, and was equipped with a floating collar to ensure stability and airtight sealing during deployment (Figure 1).

At each sampling location, the chamber was gently placed on the water surface and deployed for 30 minutes. Headspace gas samples (10 mL) were collected at 0, 5, 10, 15, 20, 25, and 30 minutes using gas-tight polypropylene syringes. Samples were immediately injected into pre-evacuated 10 mL glass vials sealed with butyl rubber septa and stored for laboratory analysis.

Methane concentrations were analyzed within 48 hours using a gas chromatograph equipped with a flame ionization detector (GC-FID; Agilent 7890A) and a Porapak Q column (2 m × 3 mm), with high-purity nitrogen as the carrier gas. The injector, oven, and detector temperatures were set at 120 °C, 50 °C, and 250 °C, respectively. Calibration curves were established using certified CH_4 standards ranging from 50 to 10,000 ppm, yielding coefficients of determination (R^2) greater than 0.999. Methane fluxes (F, mg m^{-2} h^{-1}) were calculated from the linear rate of increase in headspace methane concentration over time according to:

$$F = \frac{dC}{dt} \times \frac{V}{A} \times \frac{M}{R \times T} \quad (4)$$

where: dC/dt is the rate of concentration change (ppm h^{-1}), V is the chamber headspace volume (L), A is the chamber footprint area (m^2), M is the molar mass of CH_4 (16 g mol^{-1}), R is the universal gas constant (0.0821 L·atm·mol^{-1}·K^{-1}), and T is the absolute temperature (K).

The assumption of linear concentration increase was evaluated for each deployment, and only flux estimates with $R^2 > 0.90$ were retained for subsequent analysis to ensure data reliability. Hourly methane fluxes were converted to daily rates (mg m^{-2} d^{-1}) by multiplying by 24 for consistency with result presentation and inter-pond comparisons.

Figure 1. Gas sampling in POME ponds

Pond-wide methane emission rate

To account for differences in pond size under continuous-flow operation, a pond-wide methane emission rate was estimated by scaling the mean areal methane flux by pond surface area:

$$E_{pond} = F \times A \quad (5)$$

where: E_{pond} is the total methane emission from an individual pond (mg d^{-1}), F is the mean CH_4 flux expressed on a daily basis (mg m^{-2} d^{-1}), and A is the pond surface area (m^2).

This metric integrates spatial variability in flux with pond geometry and provides a pond-scale estimate of methane release that complements areal flux comparisons.

Although E_{pond} does not explicitly incorporate hydraulic inflow (Q) and therefore does not represent a true surface loading rate, it serves as a practical geometry-scaled proxy for evaluating the relative contribution of individual ponds to total methane emissions under steady operational conditions. This approach is particularly useful where detailed flow records are unavailable, allowing emission interpretation to explicitly consider pond size and operational scale.

Water quality analysis

Concurrent with methane flux measurements, surface water samples were collected at approximately 30 cm depth using pre-cleaned 1 L polyethylene bottles to characterize water-quality conditions influencing methanogenic processes. Samples were stored in insulated cool boxes at 4 °C immediately after collection and analyzed within 24 hours to minimize physicochemical alteration.

Three key water-quality parameters were quantified to represent complementary biogeochemical controls on methane production. Total suspended solids (TSS) were determined gravimetrically following APHA Standard Method 2540D, using pre-combusted Whatman GF/C filters (0.45 μm). Filters were dried at 105 °C for 24 hours and weighed to the nearest 0.1 mg to estimate particulate-associated substrates and potential micro-anaerobic niches. Chemical oxygen demand (COD) was measured using the standard dichromate reflux method with H_2SO_4–$K_2Cr_2O_7$ digestion and spectrophotometric detection at 600 nm, representing the total oxidizable organic fraction in the effluent. Ammonia nitrogen (NH_3–N) was quantified using the indophenol blue method with absorbance measured at 640 nm, serving as an indicator of nitrogen mineralization and buffering capacity. At the near-neutral pH conditions typical of POME, NH_3–N predominantly occurs as NH_4^+ and therefore reflects dissolved inorganic nitrogen availability relevant to methanogenic activity.

All analyses were performed in triplicate, including reagent blanks and calibration standards, to ensure analytical accuracy and precision. Quality assurance and quality control procedures followed the Standard Methods for the Examination of Water and Wastewater (Bridgewater et al., 2017).

Data processing and statistical analysis

All measurements were summarized as mean ± standard deviation (SD). Differences in water-quality parameters and methane fluxes among ponds were evaluated using one-way analysis of variance (ANOVA), followed by Tukey's honestly significant difference (HSD) post-hoc test at a significance level of $p < 0.05$. Prior to ANOVA, data distributions were visually inspected and tested for approximate normality and homogeneity of variances to confirm test assumptions.

To explore potential emission drivers, Pearson correlation analysis was used to assess bivariate relationships between methane flux and individual water-quality variables (TSS, COD, and NH_3–N). In addition, multiple linear regression was applied to identify dominant predictors of methane emissions and to evaluate their combined explanatory power. Where appropriate, variables were log-transformed to improve linearity and stabilize variance. Variance inflation factors (VIFs) were calculated to assess multicollinearity among predictors, with VIF values < 5 indicating acceptable independence.

All statistical analyses and graphical visualizations were performed using R software (version 4.5.1). Core statistical procedures were conducted using the packages *car*, *stats*, and *MuMIn*, while data handling and visualization were supported by *tidyverse*, *ggplot2*, *ggpubr*, *corrplot*, *reshape2*, *lme4*, and *networkD3*. The integration of spatially explicit sampling, multivariate statistical analysis, and process-based interpretation provided a robust analytical framework for linking pollutant removal efficiency, water-quality transformations, and methane emission dynamics within the POME pond system.

RESULT

Methane flux variability across pond stages

The selected ponds represent distinct treatment stages with substantially different surface areas and operational volumes (Table 1). Given the uniform mean water depth (4 m), pond volume scaled directly with surface area, ranging from 8.7×10^3 m³ (Pond 2) to 3.46×10^4 m³ (Pond 8). This geometric gradient provides an engineering context for interpreting spatial variations in water quality and methane emissions along the treatment train, as larger downstream ponds generally offer greater buffering capacity and potentially longer effective retention under continuous-flow operation.

Methane fluxes (CH_4) varied significantly among ponds (Figure 2). The highest mean areal flux was observed in Pond 2 (early anaerobic stage; 4,931.3 mg m^{-2} h^{-1}), followed by Pond 1 (3,523.5 mg m^{-2} h^{-1}), while substantially lower fluxes occurred in Pond 8 (2,758.5 mg m^{-2} h^{-1}) and Pond 5 (1,799.5 mg m^{-2} h^{-1}). One-way ANOVA confirmed that differences among ponds were statistically significant ($p < 0.05$), as indicated by distinct letter groupings (a–d) in Figure 2. This spatial pattern reflects a transition from strongly anaerobic, methanogenesis-dominated conditions in upstream ponds toward increasingly oxidative and substrate-limited environments in downstream treatment stages.

Pond-scale methane emissions

Although areal methane fluxes declined downstream (Figure 2), scaling fluxes by pond surface area revealed a contrasting pattern at the pond scale (Table 2). When expressed as pond-wide methane emissions (E_{pond}), Pond 8 exhibited the highest total methane release (572.09 kg d^{-1}), despite having a lower areal flux than Pond 2. This outcome reflects the large surface area of Pond 8, which amplifies total emissions under continuous operation.

In contrast, Pond 2, while displaying the highest areal methane flux, contributed a smaller pond-wide emission (258.53 kg d^{-1}) due to its comparatively limited surface area. Intermediate values were observed for Pond 1 (280.40 kg d^{-1}) and Pond 5 (274.24 kg d^{-1}). These results demonstrate that pond geometry strongly modulates total methane emissions, and that mitigation strategies based solely on areal fluxes may underestimate the contribution of large downstream ponds within multi-pond POME treatment systems.

COD and methane flux dynamics

Consistent with the spatial decline in methane fluxes, chemical oxygen demand (COD) concentrations decreased markedly along the treatment train (Figure 3a). The highest COD levels were observed in the upstream ponds, with maximum

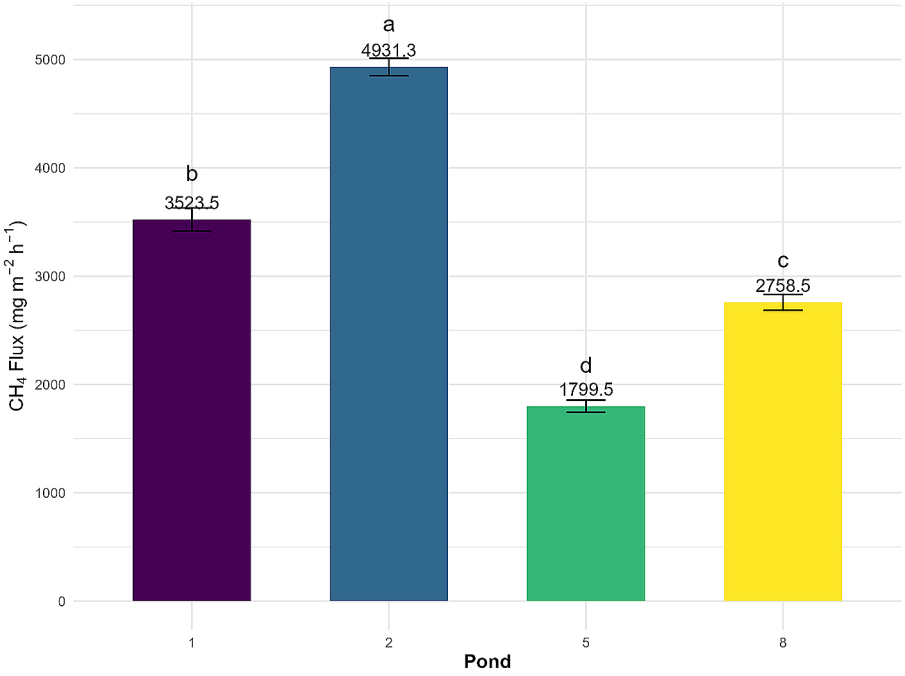

Figure 2. Mean CH_4 flux by pond

Table 2. Pond-wide methane emissions derived from areal fluxes (Figure 2) and GIS-based pond areas

Pond	Mean CH_4 flux, F (mg m^{-2} h^{-1})	Area, A (m^2)	Mean CH_4 flux (mg m^{-2} d^{-1})	Epond (mg d^{-1})	Epond (kg d^{-1})
1	3,523.5	3,315.78	84,564.0	280,395,620	280.40
2	4,931.3	2,184.41	118,351.2	258,527,545	258.53
5	1,799.5	6,349.85	43,188.0	274,237,322	274.24
8	2,758.5	8,641.35	66,204.0	572,091,935	572.09

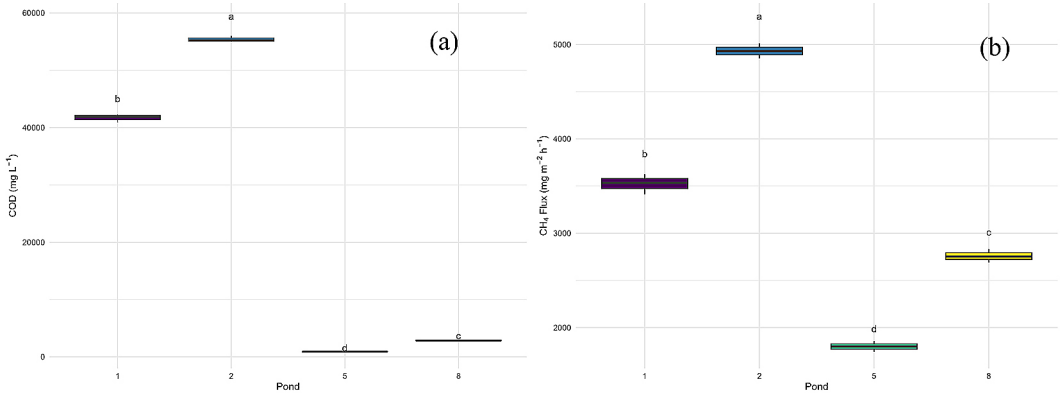

Figure 3. COD and CH_4 flux trend across pond system

concentrations in Pond 2, followed by Pond 1, while substantially lower COD concentrations occurred in the downstream ponds (Pond 5 and Pond 8). One-way ANOVA confirmed that COD concentrations differed significantly among ponds ($p < 0.05$), indicating progressive organic matter removal across successive treatment stages.

In parallel, methane fluxes exhibited a declining trend from upstream anaerobic ponds toward downstream polishing ponds (Figure 3b), reflecting reduced methanogenic activity under increasingly oxidative and substrate-limited conditions. However, despite this general co-decreasing pattern, the relationship between COD concentration and methane flux was not proportional across ponds. Notably, Pond 2 displayed the highest methane flux despite not having the highest COD concentration, whereas downstream ponds with measurable residual COD showed substantially lower CH_4 emissions.

Correlation analysis of water quality and methane flux

The relationships between water-quality parameters and methane fluxes are summarized in Figure 4 using a Pearson correlation heatmap. Methane flux exhibited a strong positive correlation with ammonia nitrogen (NH_3–N; $r > 0.8$) and with total suspended solids (TSS; $r > 0.7$), indicating that nitrogen availability and particulate-associated substrates are closely linked to methane production across the pond system. In contrast, the correlation between methane flux and chemical oxygen demand (COD) was weaker and negative, reinforcing that bulk organic load alone does not adequately explain methane emission patterns.

The strong CH_4–NH_3–N association suggests that ammonification intensity and nitrogen-driven microbial processes play a central role in regulating methanogenesis under tropical POME conditions. Ammonia nitrogen reflects the extent of protein degradation and nitrogen mineralization, processes that generate methanogenic precursors and contribute to buffering capacity favorable for methanogenic Archaea. Similarly, the positive correlation between CH_4 flux and TSS highlights the importance of particulate organic matter, which provides both fermentable substrates and micro-anaerobic niches that sustain methanogenic consortia even under partially oxidative conditions.

By contrast, the weak inverse relationship between CH_4 flux and COD supports the interpretation that COD integrates heterogeneous organic fractions, including refractory components that are poorly convertible to methane or are preferentially utilized through non-methanogenic

respiratory pathways. Together, these correlation patterns indicate that methane emissions in POME pond systems are governed more strongly by substrate bioavailability and nitrogen-associated microbial dynamics than by total organic content, providing a mechanistic explanation for the non-linear COD–CH_4 relationships observed along the treatment gradient.

Figure 4. Pearson correlation heatmap showing relationships among total suspended solids (TSS), chemical oxygen demand (COD), ammonia nitrogen (NH_3–N), and methane flux (CH_4). Color intensity indicates correlation strength (r), with positive values shown in blue.

Bivariate relationships between methane flux and water-quality parameters

Bivariate relationships between methane flux and individual water-quality parameters are presented in Figure 5. At the bivariate level, methane flux showed a strong positive association with COD (Figure 5a; $R = 0.93$, $p = 1.3 \times 10^{-5}$), indicating that ponds receiving higher organic loads also tended to exhibit higher methane emissions. This pattern reflects the role of organic matter availability in supporting anaerobic microbial metabolism under upstream pond conditions.

Similarly, methane flux was positively correlated with TSS (Figure 5b; $R = 0.91$, $p = 5.1 \times 10^{-5}$), suggesting that particulate-associated organic matter and suspended solids contribute to enhanced methanogenic activity. Suspended solids likely provide both fermentable substrates and micro-anaerobic niches that facilitate methane production within the water column.

The strongest bivariate relationship was observed between methane flux and ammonia nitrogen (NH_3–N) (Figure 5c; $R = 0.96$, $p = 6.3 \times 10^{-7}$). Methane emissions increased consistently with rising ammonia concentrations, highlighting the dominant role of nitrogen mineralization and ammonification processes in regulating methanogenesis across the pond system. Elevated NH_3–N reflects intensified protein degradation and enhanced buffering capacity, both of which favor methanogenic activity.

Importantly, while COD exhibited a positive relationship with methane flux at the bivariate level, subsequent multivariate regression analysis revealed a negative COD coefficient when controlling for TSS and NH_3–N. This divergence indicates that the apparent positive COD–CH_4 relationship is partly driven by collinearity with particulate matter and nitrogen availability, and that bulk COD alone does not represent effective substrate bioavailability for methanogenesis. Together, these results demonstrate a hierarchy of controls on methane emissions (NH_3–N > TSS > COD) once interacting water-quality factors are jointly considered.

Carbon mass balance between COD removal and methane emission

The carbon mass balance analysis presented in Figure 6 demonstrates that, despite substantial organic matter removal along the POME treatment train, only a minor fraction of removed carbon was converted into methane (CH_4–C). When expressed on a carbon basis, the amount of CH_4–C emitted was markedly lower than the total COD removed, indicating that methanogenesis accounted for only a limited share of the overall carbon transformation.

The large discrepancy between COD removal and CH_4–C emission implies that most organic carbon was processed through non-methanogenic pathways, including oxidation to CO_2, incorporation into microbial biomass, and persistence as slowly biodegradable or refractory organic matter. This finding is consistent with the observed decline in methane fluxes along downstream ponds, where increasing oxygen availability and microbial competition favor aerobic and facultative metabolic pathways over methanogenesis.

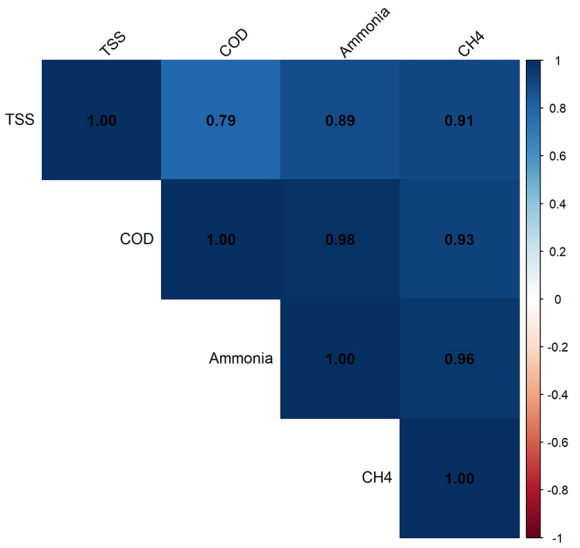

Figure 4. Correlation heatmap of water quality and CH_4 flux

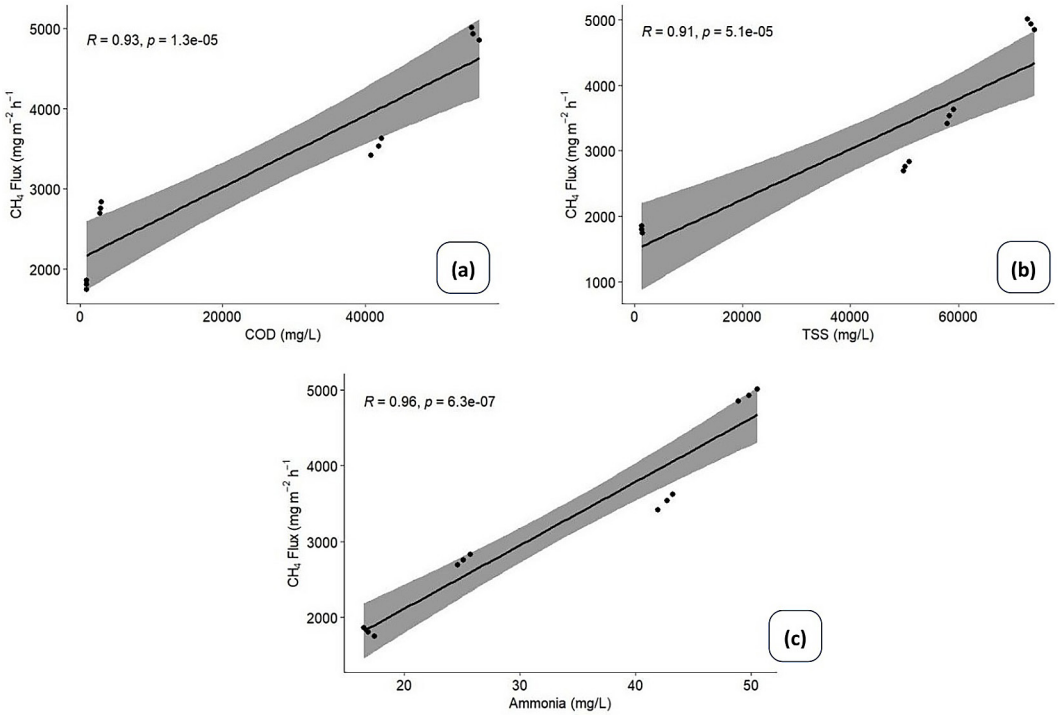

Figure 5. Bivariate relationships between methane flux and water-quality parameters: (a) CH_4 flux versus COD, (b) CH_4 flux versus TSS, and (c) CH_4 flux versus ammonia nitrogen (NH_3–N). Solid lines represent linear regression fits with shaded 95% confidence intervals

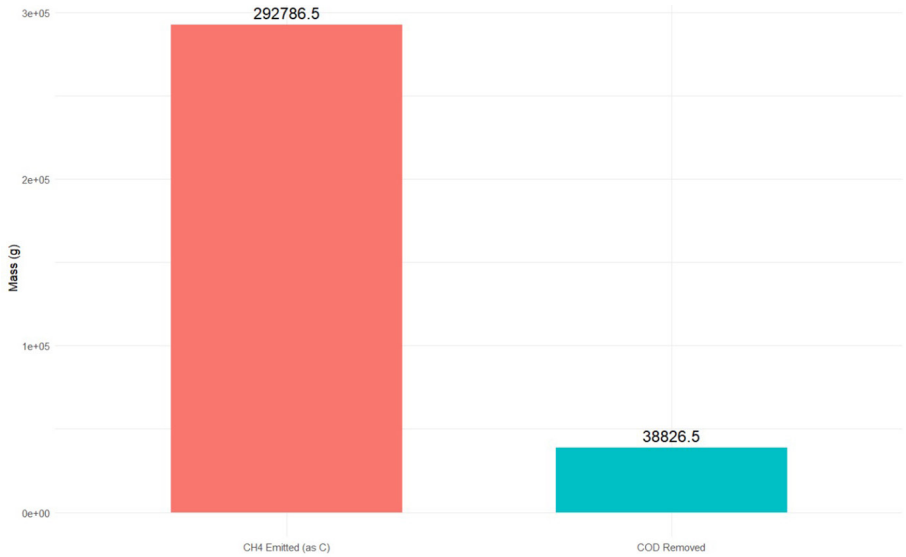

Figure 6. Comparison of total COD removal and methane carbon (CH_4–C) emission, illustrating that only a small fraction of removed organic carbon is released as methane, while the majority is processed via non-methanogenic pathways

Importantly, although CH_4–C represented a relatively small proportion of the total carbon removed, its climatic significance remains disproportionate due to the high global warming potential of methane. Thus, even modest fractions of carbon diverted toward methanogenesis can contribute substantially to greenhouse gas emissions from POME treatment systems. These results underscore that pollutant removal efficiency and greenhouse gas mitigation are not necessarily coupled, and that effective carbon removal does not automatically translate into low climate impact.

Pollutant removal efficiency and methane response

Pollutant removal efficiencies across the POME treatment system are summarized in Figure 7. Overall, COD exhibited the highest removal efficiency (93.1%), followed by ammonia (41.0%), whereas TSS showed comparatively lower removal (13.9%). These differences reflect the progressive degradation of soluble organic matter and nitrogenous compounds along the treatment train, while a substantial fraction of suspended solids remained within the system.

The observed reductions in COD and ammonia coincided with a general downstream decline in methane fluxes, indicating that improved treatment performance is broadly associated with reduced methanogenic activity. However, the relatively low removal of TSS suggests that particulate-associated substrates may persist and continue to support methane formation under favorable anaerobic microconditions, even where bulk water quality improves.

Carbon flow partitioning and methane contribution

Carbon flow partitioning within the treatment system is illustrated by the Sankey diagram (Figure 8). The diagram shows that the majority of influent COD was removed during treatment, with most of the removed carbon directed toward non-methanogenic pathways, including oxidation to CO_2 and incorporation into microbial biomass. In contrast, methane emissions accounted for only a minor fraction of the processed carbon, consistent with the carbon mass balance results (Figure 6). These results emphasize that high COD removal efficiency does not necessarily imply low greenhouse gas impact, as a small diversion of carbon toward methanogenesis can still contribute disproportionately to climate forcing.

Trade-off between water quality improvement and methane emissions

The relationship between treatment efficiency and methane emissions is further illustrated in

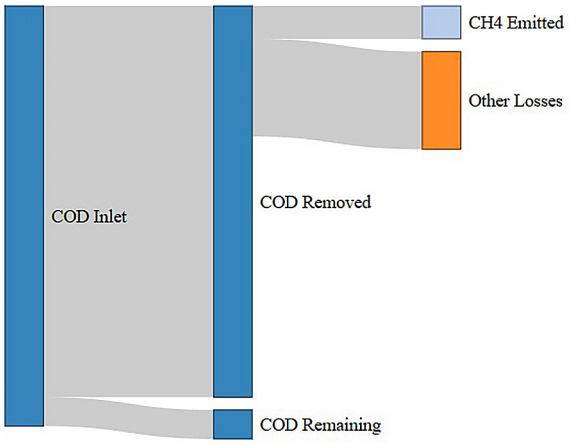

Figure 8. Sankey diagram

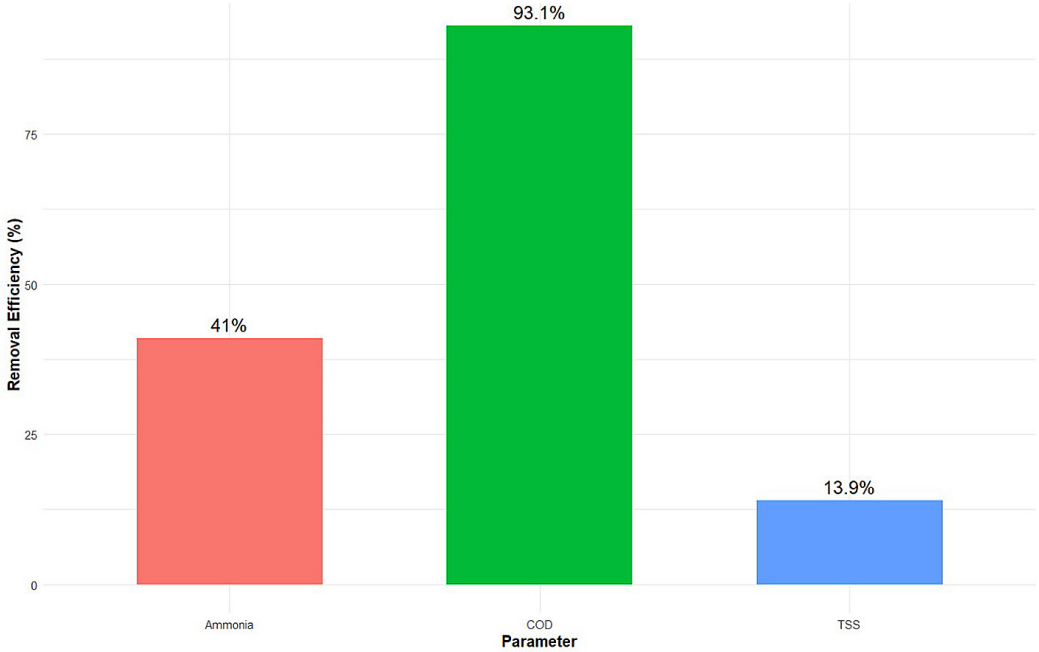

Figure 7. Pollutant removal efficiency

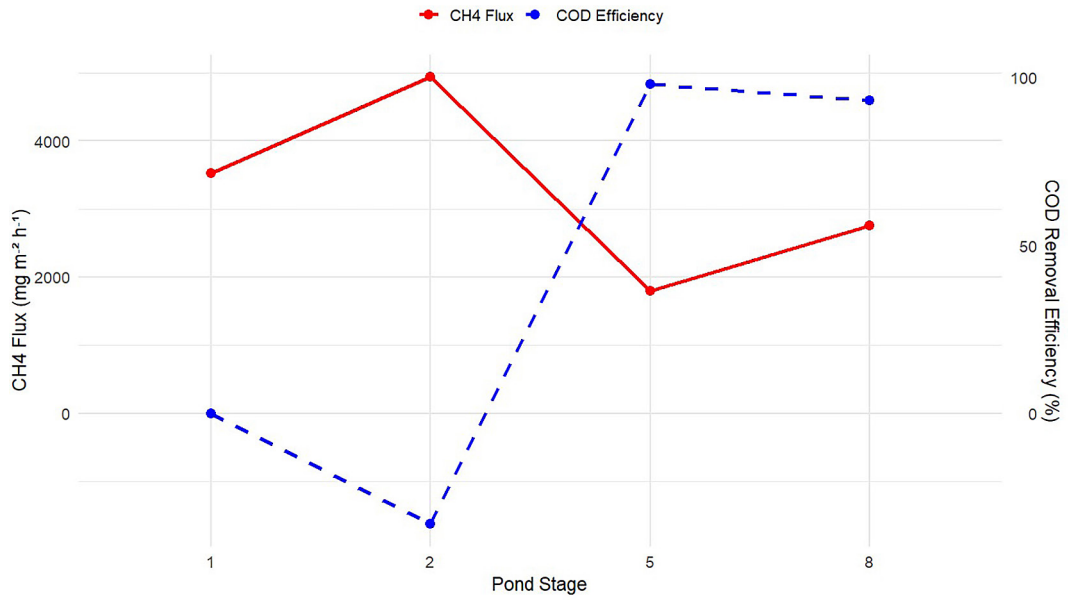

Figure 9. Trade off between water quality imporvement and CH_4 emissions

Figure 9, which depicts a trade-off between COD removal efficiency and CH_4 flux across pond stages. Upstream anaerobic ponds exhibited relatively high methane fluxes but limited COD removal, whereas downstream ponds achieved substantially higher COD removal efficiencies while emitting less methane on an areal basis.

This pattern highlights a key design dilemma in pond-based POME treatment systems: conditions that favor rapid anaerobic degradation of organic matter can also stimulate methane production, whereas increased oxidation and stabilization downstream reduce methane emissions but may shift carbon toward non-methanogenic pathways. Effective mitigation therefore requires balancing pollutant removal objectives with emission control strategies rather than optimizing either in isolation.

Multivariate controls on methane emissions

Results of the multiple regression analysis are presented in Table 3. The log-linear model explained a large proportion of the variance in methane flux ($R^2 \approx 0.90$), indicating strong predictive performance. All predictors were statistically significant ($p < 0.001$). Ammonia nitrogen emerged as the strongest positive predictor of CH_4 flux, followed by TSS, whereas COD exhibited a significant negative coefficient when controlling for the other variables. The resulting model was expressed as:

$$\log(CH_4) = 7.79 - 0.26\log(COD) + \\ + 0.0796\log(TSS) + 0.0535(NH_3 - N) \quad (6)$$

The negative COD coefficient contrasts with the positive COD–CH_4 association observed in bivariate analysis, indicating that the apparent influence of COD is mediated by its covariance with particulate matter and nitrogen availability. Once these interacting factors are accounted for, methane emissions are governed primarily by nitrogen mineralization processes and particulate-associated substrates, rather than by bulk organic load alone. This result confirms the hierarchy of methane controls identified in the correlation and bivariate analyses (NH_3–N > TSS > COD).

Table 3. Multiple regression analysis

Term	Estimate	Std. error	Statistic	P. value	Conf. low	Conf. high
(Intercept)	7.79	0.169	46.1	5.44E-11	7.4	8.18
Log (COD)	-0.26	0.0366	-7.11	1.01e- 4	-0.344	-0.176
Log (TSS)	0.0796	0.00871	9.13	1.66e- 5	0.0595	0.0997
Ammonia	0.0535	0.00474	11.3	3.41e- 6	0.0426	0.0644

DISCUSSION

This study elucidates the complex controls on methanogenesis within a tropical POME pond system, governed by interacting biogeochemical and engineering factors, particularly ammonia nitrogen (NH_4^+), TSS, and COD. The pronounced decline in CH_4 fluxes from upstream anaerobic ponds to downstream maturation ponds reflects a well-defined ecological and redox gradient, transitioning from strictly anaerobic to increasingly oxidative conditions. Under low redox potential, methanogenic Archaea dominate carbon mineralization through acetoclastic and hydrogenotrophic pathways (Mand and Metcalf, 2019; Kurth et al., 2020). In contrast, enhanced oxygen availability in facultative and maturation ponds promotes methanotrophic activity, resulting in substantial CH_4 oxidation and reduced net methane emissions (Su et al., 2022). This spatial pattern aligns with microbial succession theory in natural and engineered treatment systems, where methanogenesis is progressively replaced by aerobic and facultative processes along the treatment continuum (Yu et al., 2021).

Because the POME treatment system operates under continuous loading, methane dynamics must be interpreted within an engineering framework that integrates pond hydraulics, areal substrate delivery, and retention capacity (Lv et al., 2022). Although this study primarily relates methane fluxes to contemporaneous water-quality concentrations, pond geometry (Table 1) indicates substantial differences in buffering volume and potential hydraulic retention time (HRT) across treatment stages. In pond-based treatment systems, methane production is regulated not only by substrate concentration but also by (i) areal loading rates of COD, TSS, and nitrogen and (ii) effective retention time, which together control contact duration for hydrolysis, fermentation, and methanogenesis, as well as the development of oxidative zones downstream (Lu et al., 2023). While flow-rate data (Q) were not available during the monitoring period, the inclusion of standard loading and HRT formulations provides a reproducible analytical framework and highlights the importance of integrating routine hydraulic monitoring with greenhouse gas measurements in future POME studies (Zheng and Lam, 2024).

The incorporation of pond-wide methane emission estimates (E_{pond}) adds an engineering-relevant perspective beyond conventional areal flux comparisons. Scaling methane fluxes by pond surface area demonstrates that large downstream ponds can contribute substantially to total methane emissions despite exhibiting lower areal fluxes, a pattern also reported in waste stabilization ponds and lagoon-based wastewater systems (Rocher-Ros et al., 2023). This finding underscores that methane mitigation strategies should not rely solely on reducing fluxes per unit area, but must also explicitly consider pond geometry, surface extent, and system configuration when assessing greenhouse gas impacts in multi-pond POME treatment systems (Mahapatra et al., 2022).

From a biogeochemical standpoint, ammonia nitrogen emerged as the dominant predictor of methane flux. Ammonia reflects active ammonification and protein decomposition, supplying methanogenic precursors such as acetate, CO_2, and H_2 (Yan et al., 2020). In addition, elevated NH_4^+ concentrations enhance alkalinity and buffer pH within the optimal range for methanogenic Archaea (approximately 6.8–7.5), thereby stabilizing methanogenic activity (Park et al., 2018; Ajayi-Banji and Rahman, 2022). The strong and consistent relationship between NH_3–N and CH_4 emissions observed in this study confirms that nitrogen cycling exerts a first-order control on methane production in tropical POME systems characterized by high organic and protein loads (Chen et al., 2020).

Total suspended solids also showed a significant positive influence on methane flux. Suspended solids serve both as a reservoir of particulate organic substrates and as micro-anaerobic habitats that protect methanogenic communities from oxygen intrusion (Frehland et al., 2020). Complex organic compounds within TSS undergo hydrolysis and fermentation to produce volatile fatty acids (VFAs), which act as key intermediates for methanogenesis (Lukitawesa et al., 2020). Consequently, TSS persistence within the system can sustain methane production even as bulk water quality improves. These findings indicate that TSS control is not only critical for effluent compliance but also represents an effective lever for greenhouse gas mitigation (Lu et al., 2023).

In contrast, multivariate regression analysis revealed a significant negative association between COD and methane flux once ammonia and TSS were accounted for. This result challenges the conventional assumption of a direct linear relationship between organic load and methane production (Lv et al., 2022). Several mechanisms likely underpin this pattern. First, a substantial fraction of COD in POME consists of refractory compounds, such

as lignin-derived and humic substances, which are poorly biodegradable under anaerobic conditions (Moravia et al., 2021). Second, high-COD environments can intensify electron competition between methanogens and other microbial groups, including denitrifiers and sulfate reducers, which may suppress methanogenesis under certain redox conditions (Sela-Adler et al., 2017). Third, rapid acidogenesis under high organic loading can lead to VFA accumulation and localized pH inhibition of methanogenic Archaea (Zhang et al., 2020). These mechanisms collectively indicate that substrate bioavailability and C/N balance, rather than bulk COD alone, govern methane emission potential in POME pond systems.

Carbon mass balance analysis further demonstrated that most removed organic carbon was transformed into CO_2 and microbial biomass rather than methane. Although CH_4–C represented only a small fraction of the total processed carbon, its climatic relevance is disproportionate due to methane's high global warming potential (approximately 28 times that of CO_2 over 100 years; Noviyanto et al., 2025). The Sankey analysis confirmed that methanogenesis constitutes a minor but environmentally significant carbon pathway, consistent with previous findings in tropical pond-based treatment systems (Flickinger et al. 2020).

Finally, the trade-off analysis highlights a fundamental design dilemma in pond-based POME treatment: conditions that enhance anaerobic degradation and pollutant removal can simultaneously stimulate methane production. Effective mitigation therefore requires integrated strategies that balance treatment performance with emission control. Potential approaches include intermittent or localized aeration to enhance methane oxidation, promotion of methanotrophic biofilms, and pond design modifications that increase oxidative zones without compromising treatment efficiency (Huang et al., 2021; Zheng and Lam, 2024).

CONCLUSIONS

This study shows that methane emissions from tropical POME pond systems are governed primarily by ammonia nitrogen and TSS, while bulk COD is not a reliable predictor once interacting water-quality factors are considered. Elevated ammonia and TSS enhance methanogenesis through nitrogen mineralization, buffering effects, and particulate-associated anaerobic microhabitats, whereas COD reflects heterogeneous organic fractions with limited bioavailability.

Methane fluxes declined along the treatment continuum from anaerobic to downstream ponds, indicating a transition toward increased methane oxidation under more oxidative conditions. By integrating spatial flux measurements, pond-scale emission estimates, carbon mass balance, and multivariate analysis, this study provides a mechanistic linkage between pollutant removal, nitrogen dynamics, and greenhouse gas emissions in continuous-flow POME systems.

The identification of ammonia as the dominant regulator of methane emissions offers new insight into coupled carbon–nitrogen controls on methanogenesis in tropical wastewater treatment. These findings emphasize that high treatment efficiency does not automatically equate to low climate impact, highlighting the need to integrate nitrogen management, solids control, and methane mitigation strategies in sustainable POME treatment design.

Acknowledgements

The completion of this research and publication was made possible through the generous support of the Oil Palm Plantation Fund Management Agency (BPDPKS), Indonesia. We also extend our sincere gratitude to PT X, Indonesia, for providing access to the research location, as well as accommodation and workforce assistance, which were invaluable to the successful execution of this study.

This work was funded by the Oil Palm Plantation Fund Management Agency (BPDPKS), Indonesia, under grant number PRJ-171/DPKS/2024.

REFERENCES

1. Ajayi-Banji, A., Rahman, S. (2022). A review of process parameters influence in solid-state anaerobic digestion: Focus on performance stability thresholds. *Renewable and Sustainable Energy Reviews*, *167*, 112756. https://doi.org/10.1016/j.rser.2022.112756
2. Bridgewater, L. L., Baird, R. B., Eaton, A. D., Rice, E. W., (2017). American Public Health Association, American Water Works Association, Water Environment Federation. Standard methods for the examination of water and wastewater (23rd Edition). American Public Health Association.
3. Chen, M., Chang, L., Zhang, J., Guo, F., Vymazal, J., He, Q., Chen, Y. (2020). Global nitrogen input on

wetland ecosystem: The driving mechanism of soil labile carbon and nitrogen on greenhouse gas emissions. *Environmental Science and Ecotechnology*, *4*, 100063. https://doi.org/10.1016/j.ese.2020.100063

4. Chen, X., He, H., Zhu, N., Jia, P., Tian, J., Song, W., Cui, Z., Yuan, X. (2024). Food waste impact on dry anaerobic digestion of straw in a novel reactor: Biogas yield, stability, and hydrolysis-methanogenesis processes. *Bioresource Technology*, *406*, 131023. https://doi.org/10.1016/j.biortech.2024.131023
5. Djarot, I. N., Pawignya, H., Handayani, T., Widyastuti, N., Nuha, N., Arianti, F. D., Pertiwi, M. D., Rifai, A., Isharyadi, F., Wijayanti, S. P., Nur, M. M. A. (2024). Enhancing sustainability: Microalgae cultivation for biogas enrichment and phycoremediation of palm oil mill effluent - a comprehensive review. *Environmental Pollutants and Bioavailability*, *36*(1), 2347314. https://doi.org/10.1080/26395940.2024.2347314
6. Dominic, D., Baidurah, S. (2022). Recent developments in biological processing technology for palm oil mill effluent treatment—A review. *Biology*, *11*(4), 525. https://doi.org/10.3390/biology11040525
7. Flickinger, D. L., Costa, G. A., Dantas, D. P., Proença, D. C., David, F. S., Durborow, R. M., Moraes-Valenti, P., Valenti, W. C. (2020). The budget of carbon in the farming of the Amazon river prawn and tambaqui fish in earthen pond monoculture and integrated multitrophic systems. *Aquaculture Reports*, *17*, 100340. https://doi.org/10.1016/j.aqrep.2020.100340
8. Frehland, S., Kaegi, R., Hufenus, R., Mitrano, D. M. (2020). Long-term assessment of nanoplastic particle and microplastic fiber flux through a pilot wastewater treatment plant using metal-doped plastics. *Water Research*, *182*, 115860. https://doi.org/10.1016/j.watres.2020.115860
9. Huang, Y., Ciais, P., Luo, Y., Zhu, D., Wang, Y., Qiu, C., Goll, D. S., Guenet, B., Makowski, D., De Graaf, I., Leifeld, J., Kwon, M. J., Hu, J., Qu, L. (2021). Tradeoff of CO_2 and CH_4 emissions from global peatlands under water-table drawdown. *Nature Climate Change*, *11*(7), 618–622. https://doi.org/10.1038/s41558-021-01059-w
10. Junaidi, M. U. M., Ullah, A., Mohd Amin, N. H., Rabuni, M. F., Amir, Z., Adnan, F. H., Nafiat, N., Roslan, A. H., Othman, M. F. H., Noor Bakry, N. L. (2025). The potential of zero liquid discharge for sustainable palm oil mill effluent management in Malaysia: A techno-economic and ESG perspective. *Sustainability*, *17*(23), 10665. https://doi.org/10.3390/su172310665
11. Kacaribu, A. A., Aisyah, Y., Febriani, Darwin. (2025). Development of wastewater treatment methods for palm oil mill effluent (POME): A comprehensive review. *Resources Chemicals and Materials*, *4*(4), 100130. https://doi.org/10.1016/j.recm.2025.100130
12. Khan, I. U., Rahman, M. A., Othman, M. H. D., Iftikhar, M., Jilani, A., Mehmood, S., Shakoor, M. B., Rizwan, M., Yong, J. W. H. (2025). Innovative solutions for palm oil mill effluent treatment: A membrane technology perspective. *ACS ES&T Water*, *5*(7), 3538–3562. https://doi.org/10.1021/acsestwater.4c00432
13. Kumar, R., Basak, B., Pal, P., Chakrabortty, S., Park, Y.-K., Ali Khan, M., Chung, W., Chang, S., Ahn, Y., Jeon, B.-H. (2022). Feasibility assessment of bioethanol production from humic acid-assisted alkaline pretreated Kentucky bluegrass (*Poa pratensis* L.) followed by downstream enrichment using direct contact membrane distillation. *Bioresource Technology*, *360*, 127521. https://doi.org/10.1016/j.biortech.2022.127521
14. Kurth, J. M., Op Den Camp, H. J. M., Welte, C. U. (2020). Several ways one goal—Methanogenesis from unconventional substrates. *Applied Microbiology and Biotechnology*, *104*(16), 6839–6854. https://doi.org/10.1007/s00253-020-10724-7
15. Li, B., Sun, Y., Jiang, S., Shen, Y., Qi, Y., Zhang, G. (2024). Investigating CO_2–N_2 phase behavior for enhanced hydrate-based CO_2 sequestration. *Energy*, *289*, 129946. https://doi.org/10.1016/j.energy.2023.129946
16. Lu, H., Wang, H., Wu, Q., Luo, H., Zhao, Q., Liu, B., Si, Q., Zheng, S., Guo, W., Ren, N. (2023). Automatic control and optimal operation for greenhouse gas mitigation in sustainable wastewater treatment plants: A review. *Science of The Total Environment*, *855*, 158849. https://doi.org/10.1016/j.scitotenv.2022.158849
17. Lukitawesa, Patinvoh, R. J., Millati, R., Sárvári-Horváth, I., Taherzadeh, M. J. (2020). Factors influencing volatile fatty acids production from food wastes via anaerobic digestion. *Bioengineered*, *11*(1), 39–52. https://doi.org/10.1080/21655979.2019.1703544
18. Lv, Z., Shan, X., Xiao, X., Cai, R., Zhang, Y., Jiao, N. (2022). Excessive greenhouse gas emissions from wastewater treatment plants by using the chemical oxygen demand standard. *Science China Earth Sciences*, *65*(1), 87–95. https://doi.org/10.1007/s11430-021-9837-5
19. Mahapatra, S., Samal, K., Dash, R. R. (2022). Waste Stabilization Pond (WSP) for wastewater treatment: A review on factors, modelling and cost analysis. *Journal of Environmental Management*, *308*, 114668. https://doi.org/10.1016/j.jenvman.2022.114668
20. Mand, T. D., Metcalf, W. W. (2019). Energy conservation and hydrogenase function in methanogenic archaea, in particular the genus *Methanosarcina*. *Microbiology and Molecular Biology Reviews*, *83*(4), e00020-19. https://doi.org/10.1128/MMBR.00020-19
21. Moravia, W. G., Moreira, V. R., Lebron, Y. A. R., Lange, L. C., Santos Amaral, M. C. (2021). Influence

of humic substances on the landfill leachate biodegradability with a focus on temporal seasonality. *Water Science and Technology*, *84*(12), 3780–3790. https://doi.org/10.2166/wst.2021.499

22. Noviyanto, A., Jaya, G. I., Handru, A., Avianto, Y., Kautsar, V., Suryanti, S., Krisdiarto, A. W., Mawardi, R., Martini, T., Aziz, A. (2025). Enhancing rice productivity and mitigating greenhouse gas emissions through manure maturity and water management in paddy soils. *Journal of Ecological Engineering*, *26*(4), 313–322. https://doi.org/10.12911/22998993/200277
23. Park, J.-H., Yoon, J.-J., Kumar, G., Jin, Y.-S., Kim, S.-H. (2018). Effects of acclimation and pH on ammonia inhibition for mesophilic methanogenic microflora. *Waste Management*, *80*, 218–223. https://doi.org/10.1016/j.wasman.2018.09.016
24. Rocher-Ros, G., Stanley, E. H., Loken, L. C., Casson, N. J., Raymond, P. A., Liu, S., Amatulli, G., Sponseller, R. A. (2023). Global methane emissions from rivers and streams. *Nature*, *621*(7979), 530–535. https://doi.org/10.1038/s41586-023-06344-6
25. Sela-Adler, M., Ronen, Z., Herut, B., Antler, G., Vigderovich, H., Eckert, W., Sivan, O. (2017). Co-existence of methanogenesis and sulfate reduction with common substrates in sulfate-rich estuarine sediments. *Frontiers in Microbiology*, *8*, 766. https://doi.org/10.3389/fmicb.2017.00766
26. Su, G., Zopfi, J., Niemann, H., Lehmann, M. F. (2022). Multiple groups of methanotrophic bacteria mediate methane oxidation in anoxic lake sediments. *Frontiers in Microbiology*, *13*, 864630. https://doi.org/10.3389/fmicb.2022.864630
27. Yan, M., Treu, L., Zhu, X., Tian, H., Basile, A., Fotidis, I. A., Campanaro, S., Angelidaki, I. (2020). Insights into ammonia adaptation and methanogenic precursor oxidation by genome-centric analysis. *Environmental Science & Technology*, *54*(19), 12568–12582. https://doi.org/10.1021/acs.est.0c01945
28. Yu, J., Tang, S. N., Lee, P. K. H. (2021). Microbial communities in full-scale wastewater treatment systems exhibit deterministic assembly processes and functional dependency over time. *Environmental Science & Technology*, *55*(8), 5312–5323. https://doi.org/10.1021/acs.est.0c06732
29. Zhang, W., Li, L., Wang, X., Xing, W., Li, R., Yang, T., Lv, D. (2020). Role of trace elements in anaerobic digestion of food waste: Process stability, recovery from volatile fatty acid inhibition and microbial community dynamics. *Bioresource Technology*, *315*, 123796. https://doi.org/10.1016/j.biortech.2020.123796
30. Zheng, X., Lam, K. L. (2024). An overview of environmental co-benefits and trade-offs to reduce greenhouse gas emissions in municipal wastewater management. *Sustainable Production and Consumption*, *46*, 1–10. https://doi.org/10.1016/j.spc.2024.02.002